Metal foaming studied *in-situ* by energy dispersive X-ray diffraction of synchrotron radiation, X-ray radioscopy and optical expandometry

Dr. Catalina Jiménez[1], Dr. Francisco Garcia-Moreno[1], Beate Pfretzschner[1], B. Sc. Paul Kamm[2], B. Sc. Tillmann Robert Neu[2], Dr. Manuela Klaus[1], Prof. Dr. Christoph Genzel[1], Dr. André Hilger[1], Dr. Ingo Manke[1], Prof. Dr. John Banhart[1,2]

[1] Helmholtz Centre Berlin, Institute of Applied Materials, Hahn-Meitner-Platz 1, 14109 Berlin, Germany
[2] TU Berlin, Materials Science and Technology, Hardenbergstr. 36, 10623 Berlin, Germany

Three synchronised methods are combined for studying *in-situ* the foaming process of AlSi11 powder precursors containing either as-received TiH_2 or pre-oxidised TiH_{2-x}. The phase transformations are followed by energy dispersive X-ray diffraction of synchrotron radiation. The internal structure of the foam is monitored by X-ray radioscopy and a video camera records the overall foam expansion. Complementary mass spectrometry follows the H_2 gas release. Phase transformations of TiH_2 and TiH_{2-x} particles inside Al-Si foams are reported in this work for the first time and they are different than the ones observed for loose powders under Ar flow because the solid metal matrix initially retards H_2 outgassing, but also because after melting the liquid reacts with TiH_2 forming the ternary compounds $Ti(Al_xSi_{1-x})_2$ in the semi-solid state and $Ti(Al_{1-x}Si_x)_3$ in the liquid state of the alloy. Further reasons for the larger expansion obtained when using pre-oxidised TiH_2 are revealed as well. The oxide shell of pre-oxidised TiH_{2-x} not only shifts the onset of H_2 release towards higher temperatures, but it also hinders the reaction between blowing agent and melt, stabilizing the structure of TiH_{2-x} thus preserving its role as a good blowing agent for foaming Al-based alloys.

1 Introduction

The phase transformations of TiH_2 powder inside expanding foams and its relationship with expansion behaviour are still unknown, yet are of crucial importance for metal foaming. TiH_2 is still the most commonly used blowing agent for making Al-based foams by either powder metallurgical or melting routes.[1] Different pre-treatments were empirically optimized to shift the onset of H_2 release of TiH_2 towards higher temperatures inside the melting range of the most commonly used Al-based alloys thus obtaining larger expansion and more regular pore size foaming at ambient pressure.[2 – 6] Pressing powder mixtures under vacuum or reducing the melting temperature by alloying Al with Si, Cu, Mg, Zn or combinations of these elements are also successful strategies for producing foams of improved pore structure and properties. [7 – 14] However, the more alloyed Al is, the more complex is to predict how the decomposition of TiH_2 will be inside expanding foams.

The correlation between regimes of H_2 release and phase transformations of both as-received TiH_2 and pre-oxidised TiH_{2-x} powders under flowing Ar were recently clarified, by using a combination of *in-situ* diffraction methods, thermoanalysis and electron microscopy that helped develop core shell models to describe the decomposition of the hydride in both conditions.[15] However, studies on H_2 desorption from

foamable precursor material made for example by the powder metallurgical route, show different behaviour than the one from loose powders,[16, 4, 9] which suggests that the phase transformations of TiH_2 during foaming of Al-based alloys might be different. Therefore, experiments dedicated to study *in-situ* TiH_2 decomposition inside liquid metallic Al-based foams and its relationship with expansion are needed and motivate the present work.

2 Materials and Methods

2.1 Foamable precursor material preparation

AlSi11 precursors were prepared by the powder metallurgical route.[17] For this, silicon (Wacker Chemie GmbH, purity 99.5%), aluminium (Alpoco Ltd., purity 99.7%) and as received (AR) TiH_2 powder (Chemetall GmbH, purity 98.8 %, particle size < 36 μm) were utilised. Part of the AR TiH_2 was oxidised at 480 °C for 180 minutes in air to obtain pre-oxidised (Ox) TiH_{2-x}, which after pre-oxidation is also partially dehydrogenated.[15] Then powders were blended to prepare the alloys AlSi11 + 5 wt.% of either AR TiH_2 or Ox TiH_{2-x}. Uniaxial hot-compaction under vacuum was used to achieve metallic bonding between Al particles.[9] The vacuum atmosphere helps to remove entrapped gases and adsorbates thus obtaining a better consolidated Al matrix, which leads to produce AlSi11 foams of smaller and more uniform pore size,[9] whose foaming can be more easily followed. Tablets of 30 g mass and 36 mm diameter were consolidated inside a chamber able to keep gas pressure below 8×10^{-2} mbar. A pre-compaction step was done at ambient temperature to ensure contact between tablet and tool applying 300 MPa for 30 s. Tool and tablet were subsequently heated at 10 $K\cdot min^{-1}$ up to 400 °C, and hot-compaction was performed applying again 300 MPa for 300 s. Tablets were cut to foamable samples of $8\times8\times3$ mm^3 size. The height 3 mm matches the compaction direction.

2.2 Foaming followed by ED-XRD, optical imaging and X-ray radioscopy

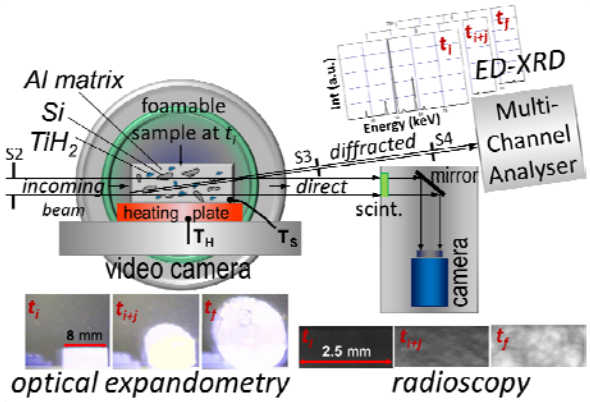

Figure 1 – Schematic side-view of the setup used for studying *in-situ* metal foaming of AlSi11 and outcome of each method. The *incoming white-beam* is partially *diffracted* and utilised for following the phase transformations by ED-XRD as a function of time. Simultaneously, radiograms of the *direct* transmitted beam obtained by radioscopy let monitor the foam structure and qualitatively the density evolution. A synchronized video camera records optical images that yield the overall foam expansion.

Figure 1 shows a schematic side-view of the experimental setup that combines ED-XRD, X-ray radioscopy and optical imaging used for studying *in-situ* the foaming process at the EDDi experimental station hosted at the synchrotron facility BESSY II of the Helmholtz Centre Berlin, in Germany. A cavity was machined onto the samples in order to insert a thermocouple and measure the sample temperature T_S. The samples were placed on the heating plate of an Anton Paar DHS 1100 furnace and a second thermocouple measured the heater temperature T_H. Foaming was conducted in air, induced by increasing T_H from 30 to 700 °C at 100 K·min^{-1}, then holding the temperature for 90 s and cooling at -100 K·min^{-1}. Additional samples were foamed heating and cooling at ± 40 K·min^{-1}, respectively.

For ED-XRD, the samples were illuminated with a white beam of X-rays of 3×1 mm^2 cross-section. The energy of diffracted photons was measured in transmission at a fixed position ($2\theta = 6°$) by a Ge multi-channel analysing detector that acquired one spectrum every 7.2 s. Thus, for a heating rate of 40 K·min^{-1} the temperature resolution is 3 K, and for 100 K·min^{-1} it is 12 K. Further features of the experimental station EDDi can be read in Ref 18.

For X-ray radioscopy, a fast PCO 1200 CMOS camera (1280x1024 pixels) was used. The X-rays were converted into visible light by applying a LuAG scintillator screen with 200 µm thickness that is suited for the high thermal loads of the white X-ray beam. The light from the scintillator was reflected by 90° by a mirror onto a Nikon Nikkor lens (200 mm) that transfers the light onto the CMOS chip. The mirror was necessary to prevent damage to the lens due to the extremely high intensity of the synchrotron X-ray beam. A 1:1 magnification was used, i.e. the pixel size in the radiographic images is identical to that of the camera (12x12 µm^2). Detector and lens were placed into a light-tight box. The achieved spatial resolution was about 30 µm and the acquisition rate was 5 frames per second (fps).

In addition, a synchronized video camera followed the overall foam expansion acquiring at 1fps. Radiographic and optical image sequences were analysed *a posteriori* with the free available software Image J.

2.3 Mass spectrometry

Hydrogen release from precursors containing either AR TiH_2 or Ox TiH_{2-x} as function of time and temperature was studied by mass spectrometry (MS) in a Netzsch 409 C thermoanalyser, which has a tubular furnace coupled via a skimmer to a quadrupole mass spectrometer. Samples, atmosphere and temperature profiles resembled those used at EDDi (described in section 2.2) but only heating and cooling at ± 40 K·min^{-1}.

3 Results

3.1 Foaming AlSi11 with as-received TiH_2

The first example of this *in-situ* study is given in Figure 2 for AlSi11 foamed with 5 wt.% AR TiH_2. Figure 2a and b contain sequences of radiograms and optical images,

respectively, at the indicated times. Both sequences show the evolution of the foam structure at particular stages of expansion, and they are linked to the complete area expansion curve by grey arrows. The superimposed curve of H_2 release represents the H_2 gas loss during foaming. In the radiogram 6 s, the sample is fully dense so the image is completely dark. But after 978 s, lighter regions (one of them indicated by an arrow) probably correspond to elongated bubbles typical of AlSi11 foams linked to crack-like pores formed in the solid state at early stages of expansion. [9] The contrast is poor due to the low expansion, so these elongated light regions can be seen more clearly in Figure 3a at 405 s which displays a similar stage of expansion. In Figure 2a after 1079 s, round lighter parts in the radiogram are better revealed as elongated bubbles (one indicated by an arrow). However, this foam remains too dense to show the foam structure clearly. The foam in the radiogram at 1600 s is even denser than at 1079 s due to shrinkage during cooling, which is also noticeable in the expansion curve.

Figure 2c is the synchronised energy dispersive map of diffracted intensities (in colour scale), which contains the principal diffraction lines of each crystalline phase whose respective (hkl) indices are indicated between brackets. The starting phases are Al (face centred cubic, Cu-type structure, s.g. $Fm\bar{3}m$ and a = 4.0497 Å), Si (face centred diamond, C-type, s.g. $Fd\bar{3}mS$ and a = 5.4307 Å), and AR TiH_2 (face centred cubic, CaF_2-type structure, s.g. $Fm\bar{3}m$ and a= 4.4509 Å). Initially, all diffraction lines move towards lower energies with increasing temperature due to thermal expansion since diffracted photon energies are inversely proportional to plane-spacing ($E \propto d^{-1}$).[18] But at 531 °C only diffraction lines of TiH_2 move towards higher energies, indicating contraction of the lattice parameter due to H_2 release.[15] The temperature 531 °C is in good agreement with the onset at 535 °C detected by MS. Melting begin is denoted in Figure 2c by the sudden increase of diffuse scattering which comes from the amorphous liquid above 585 °C on heating and 552 °C on cooling and appears as high background intensity (darker region between 900 and 1300 s). H_2 release peaks at 585 °C, i.e. when melting starts because the melt partially seals cracks. Even though H_2 release decays after melting, it remains high and expansion reaches only 196% maximum and 140% end values.

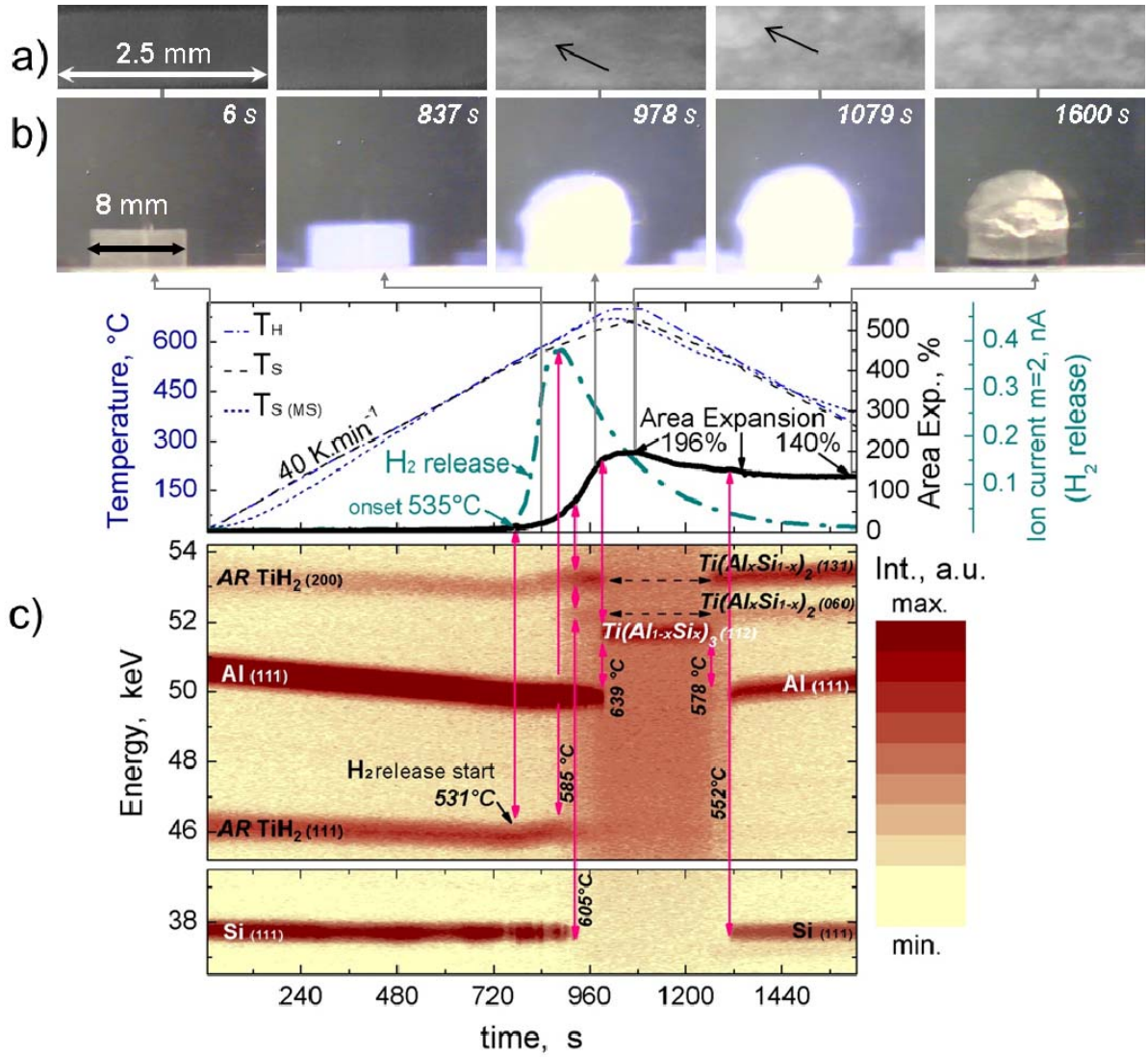

Figure 2 – a) radioscopic and b) optical image sequences synchronized with c) the energy dispersive map of diffracted intensities as function of time show pore structure evolution, expansion and diffraction lines of phases present in AlSi11 + 5 wt.% AR TiH_2 samples during foaming while applying T_H. Number triplets between brackets are hkl indices. Temperatures indicated in c) are extracted from T_S measured at the sample. H_2 release curve and respective temperature profile $T_{S\,(MS)}$ are superimposed.

When Si melts completely on heating at 605 °C, its diffraction lines disappear but lines of a new phase appear. These lines can correspond to two ternary Ti-Al-Si compounds. The first one is often referred to as τ_1, which has the general formula $(Ti_{1-y}Al_y)_8(Al_xSi_{1-x})_{16}$ where $y \approx 0.12$ and $0.06 \leq x \leq 0.25$.[19, 20] τ_1 is tetragonal of the $Zr_3Al_4Si_5$ type and s.g. $I4_1/amd$ with a = 3.576 – 3.645 Å and c = 27.15 – 28.65 Å. So, τ_1 becomes $Ti_7Al_5Si_{12}$ (a = 3.570 Å and c = 27.15 Å) for y = 0.12 and x =0.25.[19, 20] The second possible ternary compound has the same crystal structure as $TiSi_2$ (orthorrombic, $ZrSi_2$ type, s.g. $Cmcm$ with lattice parameters a = 3.541 Å, b = 13.617 Å, c = 3.576 Å) but as Al replaces partially Si the structure becomes pseudotetragonal.[20, 21] Its general formula is $Ti(Al_xSi_{1-x})_2$ with $0.15<x<0.30$ and the lattice parameters vary from a = c = 3.583 Å and b = 13.49 Å on the TiS_2 rich side to a = c = 3,611 Å whereas b remains the same on the richest Al limit.[21] $Ti(Al_xSi_{1-x})_2$ is commonly referred to as τ_2.[20] Although both silicides τ_1 and $Ti(Al_xSi_{1-x})_2$ have different crystal

structures, their most intense lines and the only visible ones in these situ experiments (due to the low counting time – 7 s – and amount of compound formed) match. Thus the diffraction map given in Figure 2c is insufficiently clear for establishing to which one of the two silicides correspond these diffraction lines.

The fading of the diffraction lines of Al at 639 °C indicates that the matrix is fully molten. Almost simultaneously the lines of $Ti(Al_xSi_{1-x})_2$ (or τ_1) disappear but lines of another ternary compound appear. This one has the general formula $Ti(Al_{1-x}Si_x)_3$ and the same structure as $TiAl_3$ (lattice parameters a = 3.857 Å and c = 8.593 Å) with Si replacing Al thus reducing the lattice parameters,[19, 22] down to a = 3.78 Å and c = 8.52 Å for the composition $Ti(Al_{0.8}Si_{0.2})_3$.[19] Soon after $Ti(Al_{1-x}Si_x)_3$ appears, the diffraction line (111) of TiH_2 faints completely. During cooling, at 578 °C the line (200) of Al reappears. It is not visible in the energy range shown in Figure 2c because this line is located around 58 keV but the same event is visible in the (111) line of Al in Figure 4c. This is the first indication that solidification starts, then the lines of $Ti(Al_{1-x}Si_x)_3$ fade whereas those of $Ti(Al_xSi_{1-x})_2$ (or τ_1) return. Solidification is complete at 552 °C when both (111) lines of Al and Si reappear. Below this temperature, all diffraction lines move towards higher energies due to thermal contraction.

If heating and cooling rates increase from ± 40 to 100 $K \cdot min^{-1}$ (see Figure 3), the foaming of AlSi11 precursors containing AR TiH_2 changes. The phase transformations given in Figure 3c are similar to the ones in Figure 2c, except for the persistence of the (111) diffraction line of TiH_2 throughout the foaming process. Besides, a milder formation of the ternary compounds $Ti(Al_xSi_{1-x})_2$ (or τ_1) and $Ti(Al_{1-x}Si_x)_3$, respectively, occurs as indicated by the lower intensity of the respective principal lines (131) of $Ti(Al_xSi_{1-x})_2$ –or (116) of τ_1, not in the Figures – and (112) of $Ti(Al_{1-x}Si_x)_3$ compared for each heating rate with the final intensity of the principal line of Al, the (111).

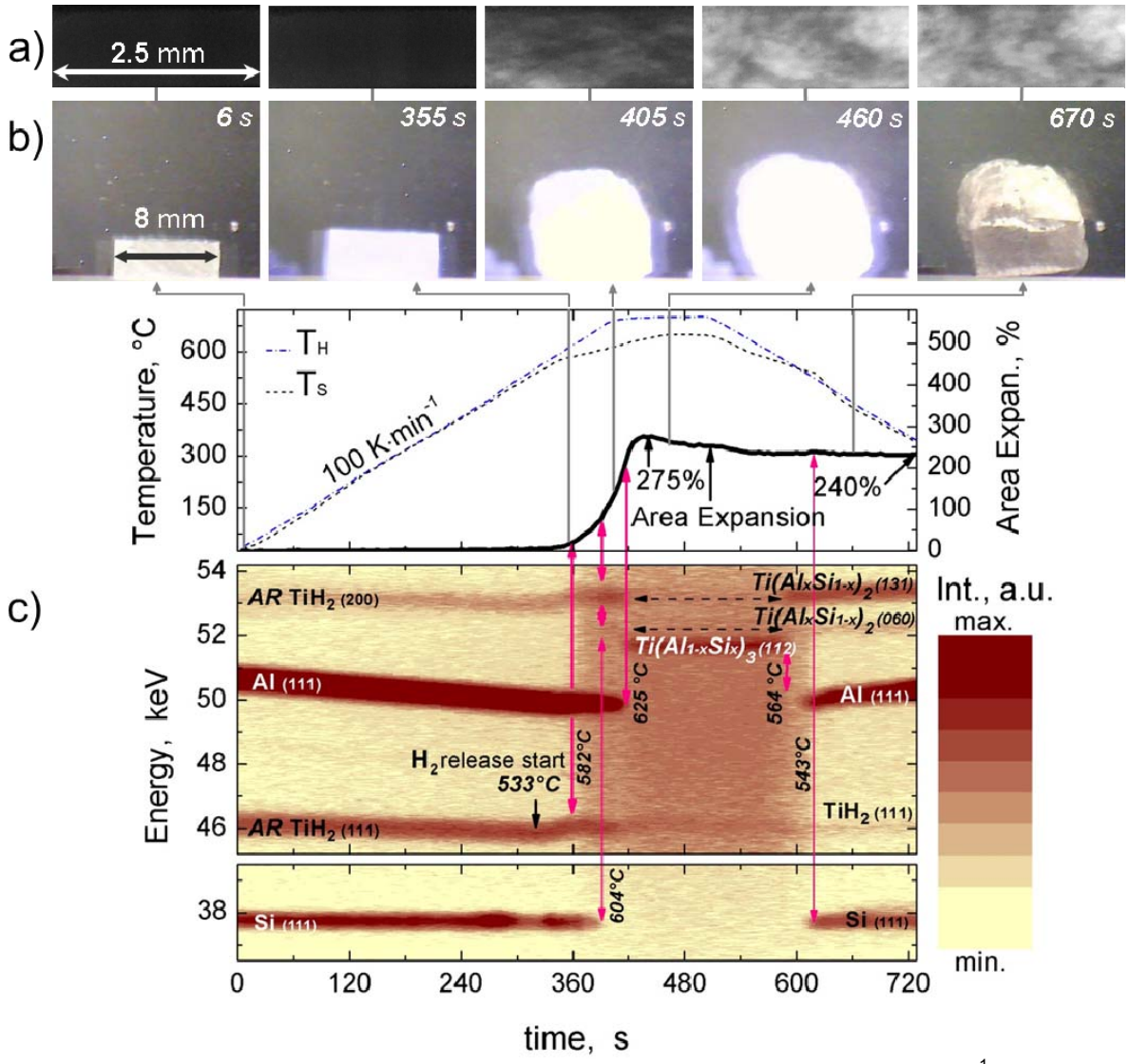

Figure 3 – Same as in Figure 2 but heating and cooling faster at ± 100 K·min^{-1}.

Events differ in absolute temperature but the differences fall within the uncertainty of the measurement since the temperature resolution is 3 K for a heating rate of 40 K·min^{-1} but 12 K for 100 K·min^{-1}. The foam shown in Figure 3 (heated and cooled at ± 100 K·min^{-1}) reaches maximum and end expansions of 275 % and 240 %, respectively, whereas the same values in Figure 2 for 40 K·min^{-1} are 196% and 140%. This means that by applying faster heating rate the foam expands more and faster cooling rate reduces shrinkage. Due to the larger expansion, the radiograms and optical images in Figure 3 a and b show better revealed striations at 405 s, bubbles at 460 s and pores at 670 s in the foam structure compared to Figure 2 a and b for different times but comparable stages of foaming.

3.2 Foaming AlSi11 with pre-oxidised TiH_{2-x}

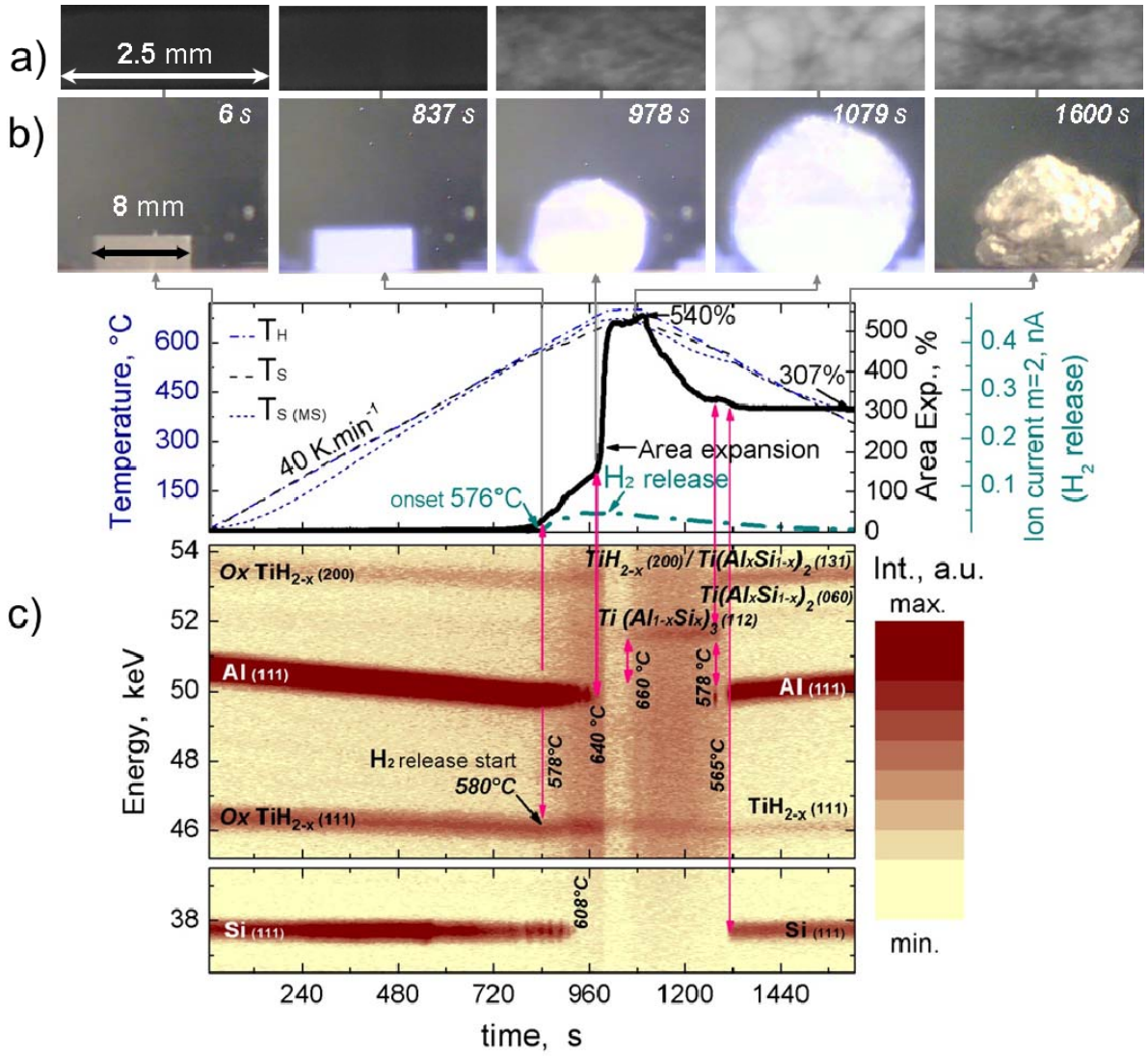

Figure 4 – Same as in Figure 2 but foaming with Ox TiH_{2-x}.

Figure 4 is the analogous of Figure 2 but for AlSi11 foamed with 5 wt.% Ox TiH_{2-x}. The diffraction lines of Ox TiH_{2-x} are located at slightly higher energies than the ones of AR TiH_2 because due to the lower hydrogen content its lattice parameter and d-spacings are smaller.[15] The diffraction lines of the oxides TiO_2 and Ti_3O that cover the oxidised hydride cannot be seen in Figure 4c because the amount of these oxides in the sample is small. However, pre-oxidation introduces significant differences regarding phase transformations, H_2 release and expansion. The move towards higher energies of the diffraction line (111) of Ox TiH_2 at 580 °C indicates the start of H_2 release. This temperature is 69 K higher than the 531 °C marked in Figure 2c for the same event when AR TiH_2 is used and matches the beginning of melting at 578 °C. The onset of H_2 release detected by MS at 576 °C is in good agreement with 580 °C too. H_2 release peaks short after Si completes melting on heating at 608 °C. The phases present in Figure 4c are the same as in Figure 2c. However the sequence is different, namely, when the diffraction line (111) of Si disappears on heating at 608 °C, the ternary compound $Ti(Al_xSi_{1-x})_2$ (or τ_1) does not appear during heating though it does during cooling from 578 °C. Neither $Ti(Al_{1-x}Si_x)_3$ forms when the

matrix melts completely at 640 °C but later, when the temperature goes up to 660 °C. All lines of the ternary compounds are less intense than in Figure 2c, which means that the formed amount is less. Also, the principal line of Ox TiH_{2-x}, the (111) remains visible throughout the foaming cycle as in Figure 3c but in Figure 4c is more intense.

The H_2 release from this sample containing Ox TiH_{2-x} is strongly reduced compared to AlSi11 foamed with AR TiH_2 (compare Figure 4 with 2). For example at the peak, the mass = 2 ion current corresponding to AlSi11 containing AR TiH_2 is 0.380 nA, whereas the same value for the sample containing Ox TiH_2 is 0.043 nA, i.e. almost 9 times smaller. Hence, this foam expands less before melting but much more after it due to the lower H_2 loss. The maximum expansion rate occurs right after Al fully melts at 640 °C, going maximum expansion up to 540 % and end expansion to 307 %, which are significantly larger than the respective 196 % and 140 % expansion values achieved in AlSi11 foaming with AR TiH_2 applying the same temperature profile. During cooling there is a little bump in the expansion curve between 578 and 545 °C, which is linked to the solidification that also involves fading of the $Ti(Al_{1-x}Si_x)_3$ structure and reprecipitation of $Ti(Al_xSi_{1-x})_2$ (or $\boldsymbol{\tau_1}$) . The larger expansion let see clearly bubbles and cell-walls inside the liquid foam in the radiogram acquired after 1079 s in Figure 4a and the denser solid resulting structure after 1600 s.

If samples containing Ox TiH_{2-x} are heated and cooled faster, the formation of ternary compounds is further inhibited and the crystalline structure on the blowing agent is more effectively retained until the end of the heating cycle as can be inferred from the intensities of diffraction lines in Figure 5c. In this sample the diffraction line (111) of Ox TiH_{2-x} is the most intense (leaving aside Al and Si) compared to all other experiments and to the ternary compounds in this experiment itself. It moves step-wise towards higher temperatures, which indicates dehydrogenation,[15] when melting starts at 579 °C, when the matrix fully melts at 604 °C, and due to increase of T_s above 615 °C after melting is complete.

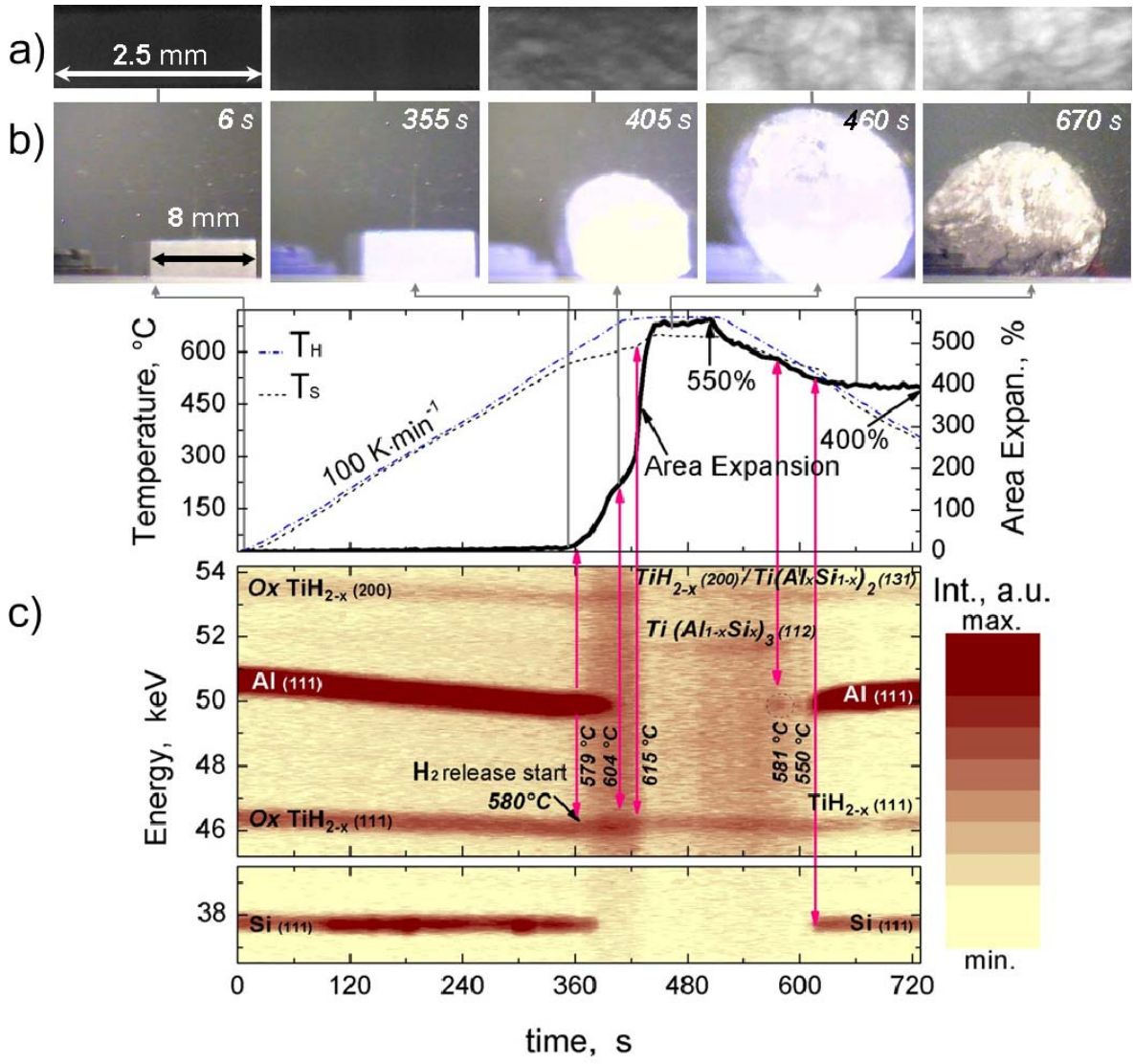

Figure 5 – Same as in Figure 4 but heating and cooling faster at ± 100 K·min^{-1}.

By heating and cooling 2.5 times faster (100 vs. 40 K·min^{-1}), maximum expansion is slightly increased from 540 % to 550 %, but shrinkage on cooling is strongly reduced. See that end expansion in Figure 5 is 400 % compared to 307 % obtained by cooling at – 40 K·min^{-1} (Figure 4). The porous structure also appears less collapsed in the radiogram after solidification (Figure 5a, 670 s). The bump in the expansion curve during cooling appears when solidification starts at 581 °C as well but is less pronounced than in Figure 4. Here this event is also linked to the fading of $Ti(Al_{1-x}Si_x)_3$ although not so clearly to the reappearance of the (131) diffraction line of $Ti(Al_xSi_{1-x})_2$ (or (116) of τ_1) because this line matches the line (200) of Ox TiH_{2-x}.

4 Discussion

4.1 Decomposition of AR TiH_2 inside liquid AlSi11 foams

The H_2 release behaviour and phase transformations of TiH_2 inside AlSi11 differ from the ones observed for cold compacted tablets under Ar flow.[23] Namely, when AR TiH_2 powder is cold-compacted and heated at 40 $K \cdot min^{-1}$, it starts to release H_2 gas at 394 °C, peaks at various temperatures to complete dehydrogenation at about 1100 °C, and the H_2 release behaviour is correlated with the following phase transformation sequence:[23]

$$\begin{cases} Heating: AR\,TiH_2 \xrightarrow{450\,^\circ C} AR\,TiH_{2-x} + \alpha \xrightarrow{510\,^\circ C} AR\,TiH_{2-x} + \alpha + \beta \\ \qquad \xrightarrow{585\,^\circ C} \alpha + \beta \xrightarrow{902\,^\circ C} \alpha \\ Cooling: \alpha\ remains \end{cases} \quad (1)$$

Where, α and β are the hexagonal closed packed (hcp) and the body centred cubic (bcc) hydrogen solid solutions of Ti.[24] No phase transformation takes place on cooling, so α is the final product of decomposition.

AlSi11 precursors containing AR TiH_2 heated at 40 $K \cdot min^{-1}$ release H_2 from 535 °C (see H_2 release curve in Figure 2). This means that the vacuum pressed Al matrix shifts the onset of H_2 release by 141 K from 394 up to 535 °C if we compare with the onset detected for cold-compacted AR TiH_2. However, this temperature shift is not sufficient to prevent strong H_2 gas losses and expansion of the precursor before melting starts, which leads not only to poor expansion but also irregular pore structure.[9] After melting, H_2 loss decreases but remains high as if the rate of H_2 production from the decomposition of the hydride is too much for the foam to entrap it and use this gas to form closed round bubbles that subsequently expand. Although the three typical stages of expansion on heating: in the solid, semi-solid and liquid state of Al-Si foams are present,[9,10] the poor expansion and the radiograms show that adding 5 wt.% AR TiH_2 is excessive for producing AlSi11 foams of good porous structure. For example, the optimized addition of TiH_2 found for AlSi7 that leads to maximum expansion and minimum shrinkage on cooling was 0.5 wt.% within the range 0 – 1 wt.%.[25] In the present study, 5 wt% added blowing agent is necessary for elucidating the phase transformation sequence, since lower blowing agent contents yield less intense diffraction peaks of the phases related to the hydride, especially the ones are only present at high temperatures. Therefore, in this work we sacrifice some foam quality, but preserve the typical expansion behaviour of the alloy and reveal the phase transformations of the blowing agent during the foaming process.

AR TiH_2 does not transform into α or β as under Ar flow, but it either reacts with the melt to form the ternary compounds $Ti(Al_xSi_{1-x})_2$ (or τ_1) and $Ti(Al_{1-x}Si_x)_3$ or it remains as the fcc hydride however more dehydrogenated than before foaming.

Centeno Sanchez et al. reported that the reaction product between molten pure Al and AR TiH_2 for the composition Al + 5wt.% AR TiH_2 after melting is $TiAl_3$.[26] But in AlSi7, Mosler and co-workers reported that the reaction layer surrounding the blowing agent particles is a Ti-Al-Si compound.[27] For clarifying whether $Ti(Al_xSi_{1-x})_2$ or τ_1 formed on cooling, one additional spectrum was acquired counting for 60 s. It revealed faint peaks more attributable to $Ti(Al_xSi_{1-x})_2$ than τ_1. However, for a liquid *L* of

eutectic composition (Al-12.6 wt. %Si), which is the case of the first liquid that forms in our sample, the invariant reaction $Al + Si \xleftrightarrow{579\,^{\circ}C} \tau_1 + L$ in the Al–Si–Ti system favours the formation of τ_1.[20, 28] Besides, for the hypoeutectic composition AlSi11 solid Al will persist above 579 °C as we observed in all ED-XRD maps. Later on heating, the calculated liquidus surface by Gröbner et al. shows that the four-phase reaction $Al + \tau_1 \xleftrightarrow{653\,^{\circ}C} Ti(Al_{1-x}Si_x)_3 + L$ should take place,[28] similar to the transition we observe when the Al matrix fully melts. The same study also mentions that the thermodynamic stabilities of τ_1 and $TiSi_2$ are similar. So if the formation of τ_1 is suppressed due to kinetic factors, one should use a metastable phase diagram which is essentially given by replacing the τ_1 phase by an enlarged $TiSi_2$ field.[28] This is more consistent with our observations because $TiSi_2$ has the same crystal structure as $Ti(Al_xSi_{1-x})_2$ as described in section 3.1. Therefore, being surrounded by a metallic matrix and then by a reactive liquid is why AR TiH_2 transforms different inside expanding AlSi11 foams than as cold-compacted powder under Ar flow. The clearest example is given in Figure 2 c because heating at 40 $K.min^{-1}$ provides the longest period of time in the present work for AR TiH_2 to react completely with the liquid at the cost of a very poor expansion. Faster heating (100 $K.min^{-1}$, Figure 3 c) leads to larger expansion not because the onset of H_2 gas release is much shifted to higher temperatures (the shift is 2 K which falls within the uncertainty of the measurement) but because the time for reaction between melt and AR TiH_2 is 2.5 times reduced. Thus, a less amount of the ternary compounds forms and the structure of the hydride along with its role of blowing agent remain for longer time.

4.2 Modification of expansion by using Ox TiH_{2-x} for foaming AlSi11

After pre-oxidation, an oxide shell mixture of the oxides Ti_3O and TiO_2, covers Ox TiH_{2-x} which is reduced in hydrogen content with respect to the AR TiH_2.[15] The onset of H_2 release from cold-compacted Ox TiH_{2-x} heated at 40 $K{\cdot}min^{-1}$ under Ar flow, occurs at 440 °C,[23] which is below the onset temperature 535 °C reported for loose Ox TiH_{2-x} powder,[15] because the cold-compaction disrupts the oxide layer.[9, 27] Dehydrogenation is complete at around 900 °C with the concomitant phase transformations:[23]

$$\begin{cases} Heating: Ox\,TiH_{2-x} + Ti_3O + TiO_2 \xrightarrow{493\text{-}500\,^{\circ}C} Ox\,TiH_{2-x} + \alpha^* + TiO_2 \xrightarrow{512\,^{\circ}C} Ox\,TiH_{2-x} \\ \qquad + \alpha^* + \beta^* + TiO_2 \xrightarrow{590\,^{\circ}C} \alpha^* + \beta^* + TiO_2 \xrightarrow{673\,^{\circ}C} \alpha^* + \beta^* \xrightarrow{721\,^{\circ}C} \alpha^* \\ Cooling: \alpha^*\ remains \end{cases} \quad (2)$$

The asterisk in α^* and β^* denotes that these hydrogen solid solutions also contain dissolved oxygen.[15]

H_2 gas release from AlSi11 precursors containing Ox TiH_{2-x} commences at 576 °C (see Figure 4 c). This means that the vacuum pressed Al matrix shifts in this case the onset by 136 K towards higher temperatures with respect to 440 °C for cold-compacted Ox TiH_{2-x} powders.[9, 23]

Pre-oxidation helps to preserve the structure of the hydride more efficiently than fast heating because the oxide layer chemically hinders the reaction with the melt, which can initially only take place on the fresh, non-oxidised surfaces created during compaction when Ox TiH_{2-x} particles break.[9, 27] Or, when TiO_2 disappears above

673 °C as indicated in sequence (2) because from 550 °C Ti_3O transforms into α^* that can reduce TiO_2.[15] So even applying relatively slow heating and cooling rates (40 $K \cdot min^{-1}$) the decomposition of Ox TiH_{2-x} and formation of ternary compounds are retarded. In Figure 4c $Ti(Al_{1-x}Si_x)_3$ appears at 660 °C and $Ti(Al_xSi_{1-x})_2$ (or τ_1) only appears on cooling when primary Al starts to solidify. The behaviour of the diffraction lines of the hydride indicates that its lattice parameter shrinks as it dehydrogenates, but it does not disappear, so it can properly act as blowing agent reducing expansion in the solid state, but increasing expansion in the two subsequent regimes: a slower one in the semi-solid state and the second after the Al matrix fully melts.

The fact that the H_2 gas loss is strongly reduced when foaming is done using Ox TiH_{2-x} instead of AR TiH_2 is not only because the onset of H_2 release is shifted towards higher temperatures matching the beginning of melting 578°C. But also because $OxTiH_{2-x}$ is consumed much slower than AR TiH_2 so the blowing agent can be activated by increasing temperature to further release gas if desired. On the one hand the use of Ox TiH_{2-x} yields much larger expansion and a better porous structure. But on the other hand, excessive remaining amount of hydride can further decompose to produce H_2 during solidification because it is an exothermic process. This, together with the change of gas diffusion losses from the foam through its outer skin during solidification, enhances a phenomenon coined as solidification expansion.[29] This solidification expansion can be seen as a bump in the expansion curve during cooling (Figure 4), which creates defects in the foams like pore-interconnections that are detrimental for the mechanical performance of the metallic foam.[30] However, solidification expansion in AlSi11 can be reduced by applying faster cooling rates as shown in Figure 5, which also reduces undesired but inevitable shrinkage and collapse of the foam.

5 Summary

The phase transformations of AR TiH_2 and Ox TiH_{2-x} inside AlSi11 metallic foams made by the powder metallurgical route were followed *in-situ* by ED-XRD for the first time. Their relationship with expansion was studied by synchronised optical expandometry and X-ray radioscopy.

Both AR TiH_2 and Ox TiH_{2-x} decompose during AlSi11 foaming undergoing different phase transformations than the ones observed for cold-compacted powders under Ar flow. In the case of AR TiH_2, initially the metallic matrix shifts the beginning of outgassing towards higher temperatures, but not high enough to prevent strong H_2 gas losses before melting of the alloy starts. This leads to unwanted expansion in the solid state. From the beginning of the alloy melting H_2 losses decrease but remain high because the liquid reacts with the hydride to form the ternary compounds $Ti(Al_xSi_{1-x})_2$ and $Ti(Al_{1-x}Si_x)_3$. This consumes the blowing agent at such a high rate that the foam cannot entrap the gas to form closed round bubbles.

But if AlSi11 is foamed with Ox TiH_2 the onset of H_2 release is shifted precisely up to the temperature when melting of the alloy starts. And also, the oxide hinders the reaction of Ox TiH_{2-x} with the melt. This preserves the crystal structure of the hydride and its role as blowing agent throughout the foaming process which leads to obtain larger expansion and better porous structure after solidification.

This combination of *in-situ* methods is especially suitable for studying the formation of high temperature phases that are not retained after cooling, thus providing an unprecedented insight into the metal foaming process and can be extended to other alloys.

We thank the European Space Agency for funding the Project AO-099-075.

6 References

[1] J. Banhart, Prog. *Mater. Sci.*, **2001**, *46*, 559.
[2] A. R. Kennedy, *Scripta Mater.*, **2002**, *47*, 763.
[3] V. Gergely and B. Clyne, *Adv. Eng. Mater.*, **2000**, *2*, 175.
[4] B. Matijasevic-Lux, J. Banhart, S. Fiechter, O. Görke, N. Wanderka, *Acta Mater.*, **2006**, *54*, 1887.
[5] D. Lehmhus, G. Rausch, *Adv. Eng. Mater.*, **2004**, *6*, 313.
[6] P. M. Proa-Flores and R. L. A. Drew, *Adv. Eng. Mater.*, **2008**, *10*, 830.
[7] A. R. Kennedy, V. R. Lopez, *Mater. Sci. Eng. A*, **2003**, *357*, 258.
[8] B. Matijasevic and J. Banhart, *Scripta Mater.*, **2006**, *54*, 503.
[9] C. Jiménez, F. Garcia-Moreno, M. Mukherjee, O. Goerke, J. Banhart, *Scripta Mater.*, **2009**, *61*, 552.
[10] I. Duarte, J. Banhart, *Acta Mater.*, **2000**, *48*, 2349.
[11] D. Lehmhus, M. Busse, *Adv. Eng. Mater.*, **2004**, *6*, 391.
[12] H.-M. Helwig, F. Garcia-Moreno, J. Banhart, *J Mater. Sci.*, **2011**, *46*, 5227.
[13] M. Lafrance, M. Isac, F. Jalilian, K.E. Waters, R.A.L. Drew, *Mater. Sci. and Eng. A*, **2011**, *528*, 6497.
[14] K. Kitazono, Y. Takiguchi, *Scripta Mater.*, **2006**, *55*, 501.
[15] C. Jiménez, F. Garcia-Moreno, B. Pfretzschner, M. Klaus, M. Wollgarten, I. Zizak, G. Schumacher, M. Tovar, J. Banhart, *Acta Mater.*, **2011**, *59*, 6318.
[16] F. von Zeppelin, M. Hirscher, H. Stanzick and J. Banhart, *Compos. Sci. Technol.*, **2003**, *63*, 2293.
[17] J. Baumeister, German Patent DE40 18 360 (**1990**).
[18] Ch. Genzel, I. Denks, J. Gibmeier, M. Klaus, G. Wagener. *Nucl. Instr. and Meth. in Phys. Res. A*, **2007**, *578*, 23.
[19] A. Raman and K. Schubert, *Z. Metallkd.*, **1965**, *56*, 44.
[20] P. Perrot, *Al-Si-Ti (Aluminium – Silicon – Titanium)* (Eds: G. Effenberg and S. Ilyenko). SpringerMaterials – Materials Science International Team MSIT® - The Landolt-Börnstein Database, DOI: 10.1007/11008514_2
[21] C. Brukl, H. Nowotny, 0. Schob and F. Benesovsky, *Monatsch. Chem.*, **1961**, *92*, 781.
[22] M. Bulanova, L. Tretyachenko, M. Golovkova and K. Meleshevich, *J Phase Equilibria and Diffusion JPEDAV*, **2004**, *25*, 209.
[23] C. Jiménez, PhD Thesis TU Berlin (**2009**)

[24] A. San Martin and F.D. Manchester, *Bull. Alloy Phase Diag.*, **1987,** *8,* 30.

[25] H.Stanzick, I.Duarte, J. Banhart, *Mat.-wiss. u. Werkstofftech.*, **2000**, *31*, 409.

[26] R. L. Centeno Sanchez, A.R. Kennedy and J.V. Wood, in: *Cellular Metals and Metal Foaming Technology* (Eds: J. Banhart, M.F. Ashby, N.A. Fleck) MIT - Verlag, Bremen, Germany **2001**.

[27] U. Mosler, A. Müller, H. Baum, U. Martin and H. Oettel, in: *Cellular Metals and Metal Foaming Technology* (Eds: J. Banhart, M. Ashby and N. Fleck) MIT-Verlag, Bremen, Germany **2001**.

[28] J. Gröbner, D. Mirković, R. Schmid-Fetzer. *Mater. Sci. Eng. A*, **2005**, *395*, 10.

[29] M. Mukherjee, F. Garcia-Moreno, J. Banhart, *Acta Mater.*, **2010**, *58*, 6358.

[30] M. Mukherjee, F. Garcia-Moreno, J. Banhart, *Scripta Mater.*, **2010**, *63*, 235.